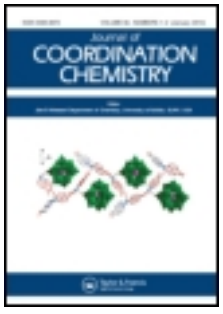

Journal of Coordination Chemistry
Publication details, including instructions for authors and subscription information:
http://www.tandfonline.com/loi/gcoo20

On the governing of alkaline earth metal nitrate coordination spheres by hexamethylenetetramine

TOMASZ SIERAŃSKI [a] & RAFAL KRUSZYNSKI [a]

[a] Institute of General and Ecological Chemistry, Technical University of Lodz , Lodz , Poland

Accepted author version posted online: 06 Nov 2012.Published online: 11 Dec 2012.

To cite this article: TOMASZ SIERAŃSKI & RAFAL KRUSZYNSKI (2013) On the governing of alkaline earth metal nitrate coordination spheres by hexamethylenetetramine, Journal of Coordination Chemistry, 66:1, 42-55, DOI: 10.1080/00958972.2012.744835

To link to this article: http://dx.doi.org/10.1080/00958972.2012.744835

Journal of Coordination Chemistry
Vol. 66, No. 1, 10 January 2013, 42–55

On the governing of alkaline earth metal nitrate coordination spheres by hexamethylenetetramine

TOMASZ SIERAŃSKI and RAFAL KRUSZYNSKI*

Institute of General and Ecological Chemistry, Technical University of Lodz, Lodz, Poland

(*Received 17 July 2012; in final form 14 September 2012*)

Alkaline earth metal nitrate coordination compounds with hexamethylenetetramine, $[Mg(H_2O_6)]^{2+} \cdot 2NO_3^- \cdot 2hmta \cdot 4H_2O$(**1**), $[Ca_2(H_2O)_6(NO_3)_4] \bullet 2hmta$(**2**)and $[Sr_2(H_2O)_8(NO_3)_4] \bullet 2$ hmta (**3**)]], have been synthesized and characterized by elemental and thermal analysis, IR spectroscopy, and X-ray crystallography. Introduction of hmta to the outer coordination sphere allows changing of the inner coordination sphere giving the dinuclear coordination compounds of calcium and strontium nitrates. The compounds are air stable at room temperature and soluble in water. The ions and molecules are assembled via O–H···O, O–H···N and C–H···O hydrogen bonds. Thermal analyses show crucial differences in decomposition processes (especially in the case of **3** that finally decomposes to the mixture of SrO and $Sr(NO_3)_2$). The IR spectrum of **3** shows lack of NO_3^- bending vibration (present in the spectra of the respective pure salts at 741–759 cm^{-1}), while in **2** this band is weakened and shifted to lower frequencies. Only the IR spectrum of **3** clearly exhibits bands originating from NO_3^- overtones and combination bands (in the spectral range 2073–2474 cm^{-1}).

Keywords: Magnesium; Calcium; Strontium; Hexamethylenetetramine; Thermal decomposition; IR spectroscopy

1. Introduction

Bonding in metal–ligand systems is an active area of research due to their potential applications in fields such as biochemistry and environmental chemistry [1–6]. Especially, alkaline earth metal chemistry is of interest [7–16]. Magnesium and calcium are most studied but heavier alkaline earth metals are also investigated. For instance, after the development of the strontium-based drug – strontium renelate – which reduces the incidence of fractures in osteoporotic patients, an increasing awareness of this metal's role in humans has grown [17, 18]. Nevertheless, when comparing to transition metal coordination compounds, the ones of alkaline earth metals have not been so widely studied [19]. Dinuclear and multinuclear coordination compounds [20–25] may exhibit interesting properties, for instance catalytic ones, and study of interactions that appear in their structures can help to understand the processes of self-organization that are very important in modern nanotechnology and supramolecular chemistry [26–29]. Thus, investigation of alkaline earth metal coordination chemistry is essential for obtaining new bioactive compounds with clinical applications and for new materials. Such materials should be environmentally and human friendly and their syntheses should be simple and low-priced. Additionally, research of

*Corresponding author. Email: rafal.kruszynski@p.lodz.pl

ISSN 0095-8972 print/ISSN 1029-0389 online
http://dx.doi.org/10.1080/00958972.2012.744835

coordination chemistry concerning this metal group may help to learn about their binding mechanisms to bioactive molecules (e.g. nucleic acids, proteins, amino acids). As a model ligand, hexamethylenetetramine (hmta) was chosen. It is a strong and bulky organic base potentially tetradentate due to four N-donors [30] that is commercially available, inexpensive and has many applications ranging from use in phenolic resins [31, 32] to clinical applications (e.g. hmta is used for treating urinary tract infections) [33]. This ligand can be utilized as an outer coordination sphere modulator of the inner coordination sphere [34] and can be used as a crosslinking agent in binuclear and multinuclear coordination compounds [35–37]; hmta is also used as a model for bioactive molecules (mentioned above) and some coordination aspects of alkaline earth metal coordination compounds may pertain to other bioactive molecules. Considering the important role of alkaline earth metals, magnesium, calcium, and strontium nitrate coordination compounds with hmta were synthesized and studied. The hmta (located in the outer coordination sphere) modulated the inner coordination sphere giving dinuclear coordination compounds of calcium and strontium (typically these metals form polymeric compounds or mononuclear molecular coordination compounds). The thermal properties study (including stability and decomposition) was undertaken because it can help to learn about the optimum conditions of compound synthesis and permissible storage parameters. These studies are also important in the aspect of solid, pharmacologically active, compounds (used in medicine), that typically are prepared at temperatures higher than ambient ones [38]. Undertaken IR spectroscopy studies are significant in terms of vibrational structure properties [39–41].

2. Experimental

2.1. *Materials and syntheses*

All chemicals (analytical grade) were obtained from POCh SA and used without purification. Alkaline earth metal oxides (0.0090 g and 0.1120 g, respectively, for magnesium and calcium oxides) were dissolved in small amounts of water – about 5 cm^3. For strontium, its carbonate was used (0.2960 g). Then, nitric acid (0.143 cm^3 of 13.99 mol L^{-1} solution) was added to each solution (acid to metal molar ratio 1 : 1). The solutions were mixed for several minutes on a magnetic stirrer and filtered to separate them from the unreacted alkaline earth metal oxide/hydroxide/carbonate excess. The filtrates were mixed with aqueous solutions of hexamethylenetetramine (molar ratio 1 : 1; 0.1402 g of hexamethylenetetramine dissolved in 5 cm^3 of water). The mixtures were placed in a refrigerator and left to crystallize at 5 °C. After three weeks, the obtained crystals were filtered and dried in air. The analogous reaction between barium carbonate, nitric acid, and hmta always leads to almost quantitative crystallization of barium nitrate from the solution.

2.2. *Physical measurements*

IR spectra were recorded on a FTIR Jasco 6200 spectrometer in the spectral range 4000–400 cm^{-1} as KBr pellets. Thermal analyses were carried out in a TG-DTA-SETSYS-16/18 thermoanalyzer coupled with a ThermoStar (Balzers) mass spectrometer and FTIR Jasco 6200 spectrometer. The samples were heated in corundum crucibles up to 1000 °C at 5 °C min^{-1} in synthetic air (20% O_2 and 80% N_2) flow. The solid products of thermal decomposition were determined from derivatographic curves and on the basis of IR spectra and elemental analyses of the sinters. The final and some products of the decomposition were

confirmed by X-ray powder diffraction (XRPD) using the Powder Diffraction File [42]. The volatile products of decomposition were studied by mass and IR spectrometry. The temperature ranges of the processes were determined by thermoanalyzer Data Processing Module [43]. Elemental analyses were carried out using a Vario EL III CHNOS Elemental Analyzer (C, H, N, O, S). Alkaline earth metal contents (magnesium, calcium, and strontium) were determined by complexometric titration using EDTA [44]. Ammonium ions (formed as a result of acidic decomposition of hmta) and nitrate ions were determined by Nessler method (a sample mineralized in an acidic environment) and by brucine method, respectively. Elemental analyses for the compounds [calculated/found (%)] (**1**) : C 23.67/23.69; H 7.23/7.20; O 42.04/41.95; N 23.01/23.05; Mg 3.99/4.11; (**2**) : C 20.11/20.19; H 5.02/5.06; O 40.18/40.06; N 23.46/23.46; Ca 11.18/11.10; (**3**) : C 17.00/16.94; H 4.72/4.71; O 37.74/37.69; N 19.83/19.81, Sr 20.67/20.80.

2.3. *X-ray crystallography*

Colorless rectangular prism-shaped crystals were mounted in turn on a KM-4-CCD automatic diffractometer equipped with a CCD detector and used for data collection. X-ray

Table 1. Crystal data and structure refinement details for **1–3**.

Compound	**1**	**2**	**3**
Empirical formula	$C_{12}H_{44}MgN_{10}O_{16}$	$C_{12}H_{36}Ca_2N_{12}O_{18}$	$C_{12}H_{40}Sr_2N_{12}O_{20}$
Formula weight	608.88	716.69	847.80
Crystal system, space group	Monoclinic, $P2_1/n$	Monoclinic, $P2_1/n$	Monoclinic, $P2_1/c$
Temperature [K]	291.0(3)	291.0(3)	291.0(3)
Wavelength	0.71073	0.71073	0.71073
Unit cell dimensions [Å, °]	$a = 9.4350(3)$	$a = 6.8846(2)$	$a = 13.4829(5)$
	$b = 16.1263(5)$	$b = 17.5589(5)$	$b = 11.1146(3)$
	$c = 19.2962(5)$	$c = 12.7118(4)$	$c = 12.1431(4)$
	$\beta = 90.572(2)$	$\beta = 101.412(3)$	$\beta = 116.755(4)$
Volume [Å^3]	2935.80(15)	1506.69(8)	1506.69(8)
Z, Calculated density [Mg m^{-3}]	4, 1.378	2, 1.580	2, 1.733
Absorption coefficient [mm^{-1}]	0.143	0.473	3.378
F(000)	1304	752	864
Crystal size [mm]	0.389 × 0.291 × 0.227	0.209 × 0.194 × 0.155	0.287 × 0.234 × 0.045
Θ Range for data collection [°]	1.65 to 25.02	2.0 to 25.02	1.69 to 25.02
Index ranges	$-9 \le h \le 11$,	$-8 \le h \le 8$,	$-16 \le h \le 16$,
	$-18 \le k \le 19$,	$-20 \le k \le 20$,	$-12 \le k \le 13$,
	$-22 \le l \le 22$	$-15 \le l \le 15$	$-14 \le l \le 14$
Reflections collected/ unique	29,068/5177 [$R_{(int)} = 0.0267$]	15,073/2659 [$R_{(int)} = 0.0352$]	16,004/2860 [$R_{(int)} = 0.0278$]
Completeness	100% to Θ = 25°	100% to Θ = 25°	100% to =Θ 25°
Min. and max. transmission	0.946 and 0.972	0.912 and 0.930	0.0.394 and 0.866
Data/restraints/ parameters	5177/0/358	2659/0/199	2860/0/208
Goodness-of-fit on F^2	1.059	1.136	1.067
Final R indices [$I > 2\sigma(I)$]	$R1 = 0.0409$, $wR2 = 0.1260$	$R1 = 0.0359$, $wR2 = 0.1114$	$R1 = 0.0207$, $wR2 = 0.0563$
R indices (all data)	$R1 = 0.0538$, $wR2 = 0.1334$	$R1 = 0.0441$, $wR2 = 0.1214$	$R1 = 0.0304$, $wR2 = 0.0735$
Largest diff. peak and hole [e· Å^{-3}]	0.532 and −0.339	0.612 and −0.436	0.326 and −0.290

intensity data were collected with graphite monochromated MoK_α radiation ($\lambda = 0.71073$ Å) at 291.0(3) K with ω scan mode. The 30, 12, 16 s exposure times were used (respectively for **1**, **2**, and **3**) and reflections inside the Ewald sphere were collected up to $2\theta = 50°$. The unit cell parameters were determined from least-squares refinement of the 7041, 9861, and 6485 strongest reflections, respectively, for **1**, **2**, and **3**. Details concerning crystal data and refinement are given in table 1. Examination of reflections on two reference frames monitored after each 33.33 min showed no loss of intensity during measurements of **2** and

Table 2. Selected structural data for **1–3**.

Compound **1**		Compound **2**		Compound **3**	
Bond length [å]					
Mg1–O1	2.046(1)	Ca1–O1	2.522(2)	Sr1–O1	2.720(2)
Mg1–O2	2.051(1)	Ca1–O2	2.4416(19)	Sr1–O1^{ii}	2.683(2)
Mg1–O3	2.050(1)	Ca1–O4	2.4635(17)	Sr1–O2	2.720(2)
Mg1–O4	2.065(1)	Ca1–O4^{i}	2.4878(16)	Sr1–O4	2.691(2)
Mg1–O5	2.063(1)	Ca1–O5	2.599(2)	Sr1–O5	2.648(2)
Mg1–O6	2.055(1)	Ca1–O7	2.3542(17)	Sr1–O7	2.588(2)
		Ca1–O8	2.3342(17)	Sr1–O8	2.571(2)
		Ca1–O9	2.3189(17)	Sr1–O9	2.542(2)
				Sr1–O10	2.534(2)
Interbond angle [°]					
O1–Mg1–O3	178.92(5)	O9–Ca1–O8	76.86(7)	O10–Sr1–O9	77.93(9)
O1–Mg1–O2	88.04(5)	O9–Ca1–O7	91.48(7)	O10–Sr1–O8	146.09(8)
O3–Mg1–O2	92.91(5)	O8–Ca1–O7	81.24(6)	O9–Sr1–O8	71.22(8)
O1–Mg1–O6	92.65(5)	O9–Ca1–O2	129.85(7)	O10–Sr1–O7	136.93(7)
O3–Mg1–O6	87.91(5)	O8–Ca1–O2	150.21(7)	O9–Sr1–O7	133.92(7)
O2–Mg1–O6	87.66(5)	O7–Ca1–O2	84.72(7)	O8–Sr1–O7	76.55(7)
O1–Mg1–O5	87.30(5)	O9–Ca1–O4	113.33(7)	O10–Sr1–O5	76.53(9)
O3–Mg1–O5	92.14(5)	O8–Ca1–O4	83.30(6)	O9–Sr1–O5	82.97(8)
O2–Mg1–O5	92.24(5)	O7–Ca1–O4	146.77(6)	O8–Sr1–O5	85.92(8)
O6–Mg1–O5	179.89(6)	O2–Ca1–O4	94.66(8)	O7–Sr1–O5	126.88(7)
O1–Mg1–O4	90.94(5)	O9–Ca1–O4^{i}	154.45(7)	O10–Sr1–O1^{ii}	71.74(7)
O3–Mg1–O4	88.11(5)	O8–Ca1–O4^{i}	77.69(7)	O9–Sr1–O1^{ii}	147.55(8)
O2–Mg1–O4	178.91(5)	O7–Ca1–O4^{i}	82.46(6)	O8–Sr1–O1^{ii}	140.91(7)
O6–Mg1–O4	92.80(5)	O2–Ca1–O4^{i}	74.50(6)	O7–Sr1–O1^{ii}	68.75(6)
O5–Mg1–O4	87.30(5)	O4–Ca1–O4^{i}	65.54(6)	O5–Sr1–O1^{ii}	100.57(8)
		O9–Ca1–O1	80.46(7)	O10–Sr1–O4	110.50(9)
		O8–Ca1–O1	155.01(8)	O9–Sr1–O4	120.52(8)
		O7–Ca1–O1	89.05(9)	O8–Sr1–O4	75.05(7)
		O2–Ca1–O1	49.56(6)	O7–Sr1–O4	80.14(7)
		O4–Ca1–O1	115.66(9)	O5–Sr1–O4	46.81(8)
		O4^{i}–Ca1–O1	123.98(7)	O1^{ii}–Sr1–O4	81.66(7)
		O9–Ca1–O5	78.22(7)	O10–Sr1–O2	101.75(8)
		O8–Ca1–O5	107.29(9)	O9–Sr1–O2	71.55(7)
		O7–Ca1–O5	164.42(7)	O8–Sr1–O2	81.77(7)
		O2–Ca1–O5	92.89(10)	O7–Sr1–O2	71.99(6)
		O4–Ca1–O5	48.71(6)	O5–Sr1–O2	154.12(8)
		O4^{i}–Ca1–O5	111.79(6)	O1^{ii}–Sr1–O2	103.35(6)
		O1–Ca1–O5	77.82(10)	O4–Sr1–O2	147.16(7)
				O10–Sr1–O1	72.00(7)
				O9–Sr1–O1	98.86(7)
				O8–Sr1–O1	125.85(7)
				O7–Sr1–O1	74.44(6)
				O5–Sr1–O1	147.25(8)
				O1^{ii}–Sr1–O1	61.15(7)
				O4–Sr1–O1	140.45(7)
				O2–Sr1–O1	46.07(6)

Symmetry transformations used to generate equivalent atoms: (i) $-x+1, -y, -z+2$; (ii) $-x+1, -y+2, -z$

Table 3. Hydrogen bonds in **1–3** [Å, °].

D–H···A	d(D–H)	d(H···A)	d(D–A)	∠(DHA)
Compound **1**				
O1–H1O···O21^{i}	0.91	1.89	2.794(2)	172.4
O1–H1P···N12	0.82	2.01	2.813(2)	168.8
O2–H2O···O99^{ii}	0.89	1.86	2.741(2)	168.8
O2–H2P···N11^{ii}	0.86	1.97	2.825(2)	175.2
O3–H3O···O96^{iii}	0.88	1.84	2.716(2)	174.1
O3–H3P···N2^{iv}	0.83	1.99	2.817(2)	173
O4–H4O···O98	0.87	1.91	2.768(2)	170.1
O4–H4P···N1^{i}	0.82	2.05	2.863(2)	169.5
O5–H5O···O31^{v}	0.9	1.94	2.828(2)	167
O5–H5P···N13^{vi}	0.86	1.97	2.814(2)	170.8
O6–H6O···O97	0.84	1.9	2.735(2)	170.7
O6–H6P···N3	0.89	1.94	2.823(2)	172.4
O96–H96O···O32	0.98	1.93	2.905(3)	174.2
O96–H96P···O21^{vii}	0.99	2.03	2.986(2)	163.7
O96–H96P···O22^{vii}	0.99	2.34	3.124(3)	136.2
O97–H97O···O31^{viii}	0.9	2.37	3.139(3)	143.8
O97–H97O···O32^{viii}	0.9	2.07	2.930(3)	159.1
O97–H97P···O22	0.92	2.07	2.948(2)	159.5
O97–H97P···O23	0.92	2.51	3.294(3)	144.3
O98–H98O···N14^{iX}	0.92	1.95	2.867(2)	172.3
O98–H98P···O32^{x}	0.93	2.5	3.271(3)	140.3
O98–H98P···O33^{x}	0.93	2.26	3.114(3)	152.6
O99–H99O···N4^{xi}	0.88	1.98	2.856(2)	176.5
O99–H99P···O23	0.95	2.11	3.002(2)	157.2
C3–H3B···O33^{iii}	0.97	2.6	3.490(3)	153.4
C12–H12A···O23^{i}	0.97	3.22	3.962(3)	134.6
C15–H15B···O32^{xii}	0.97	2.57	3.366(3)	139.4
Compound **2**				
O7–H7O···O6^{xiii}	0.81	2.43	3.015(3)	130.2
O7–H7P···N14^{xiv}	0.87	1.9	2.773(3)	178.1
O8–H8O···N13^{xv}	0.87	1.89	2.758(2)	179
O8–H8P···O5^{xvi}	0.8	2.22	2.958(3)	154.7
O8–H8P···O6^{xvi}	0.8	2.5	3.217(3)	150.6
O9–H9O···N12^{xvi}	0.83	2.03	2.834(2)	163.2
O9–H9P···N11	0.87	1.9	2.774(3)	176.9
C12–H12A···O2^{xvii}	0.97	2.43	3.306(3)	150.6
C15–H15B···O3^{xviii}	0.97	2.54	3.423(3)	151.8
Compound **3**				
O7–H7O···N13^{xix}	0.83	1.95	2.786(3)	176.5
O7–H7P···N11^{xx}	0.88	1.92	2.771(3)	162.4
O8–H8O···N12^{xxi}	0.88	1.98	2.822(3)	159
O8–H8P···O5^{xix}	0.83	2.35	3.172(3)	171.8
O8–H8P···O6^{xix}	0.83	2.51	3.143(4)	133.3
O9–H9O···N14	0.93	1.9	2.813(4)	167.4
O9–H9P···O3^{xxii}	0.85	2.31	2.931(4)	130.4
O10–H10O···O7^{iv}	0.88	1.94	2.801(3)	168.6
O10–H10P···O2^{xxiii}	0.88	1.99	2.846(3)	162.3
C14–H14A···O3^{xxii}	0.97	2.53	3.135(4)	120.6
C16–H16A···O5	0.97	2.59	3.429(4)	144.7

Symmetry transformations used to generate equivalent atoms: (i) $x+1$, y, z; (ii) $-x+1$, $-y+1$, $-z$; (iii) x, y, $z-1$; (iv) $-x+1$, $-y+2$, $-z$; (v) $x+1$, y, $z-1$; (vi) $x+2$, $-y+1$, $-z$; (vii) $-0.5+x+1$, $-0.5-y+2$, $-0.5+z+1$; (viii) $-0.5+x+1$, $-0.5-y+2$, $-0.5+z$; (ix) $0.5-x+1$, $0.5+y$, $0.5-z$; (x) $-x+1$, $-y+2$, $-z+1$; (xi) $0.5-x$, $0.5+y-1$, $0.5-z$; (xii) $-0.5+x+1$, $-0.5-y+2$, $-0.5+z$; (xiii) $-x+1$, $-y$, $-z+2$; (xiv) $-x+1$, $-y$, $-z+1$; (xv) $-0.5+x$, $-0.5-y+1$, $-0.5+z+1$; (xvi) $+x-1$, $+y$, $+z$; (xvii) $0.5-x+1$, $0.5+y$, $0.5-z+1$; (xviii) $-x+2$, $-y$, $-z+1$; (xix) $+x$, $-0.5-y+2$, $-0.5+z+1$; (xx) $+x$, $+y+1$, z; (xxi) $-x+2$, $0.5+y$, $0.5-z$; (xxii) $-x+1$, $0.5+y-1$, $0.5-z$; (xxiii) $+x$, $-0.5-y+2$, $-0.5+z$

3 and 5.17% intensity decay during measurement of **1**. Lorentz, polarization, decay, and numerical absorption [45] corrections were applied. The structures were solved by direct methods. All non-hydrogen atoms were refined anisotropically using full-matrix, least-squares technique on F^2. All hydrogen atoms were found from difference Fourier syntheses after four cycles of anisotropic refinement and refined as "riding" on the adjacent atom with individual isotropic displacement factor equal 1.2 times the value of equivalent displacement factor of the patent carbon atoms and 1.5 times for patent oxygen atoms. Carbon-bonded hydrogen atoms positions were idealized after each cycle of refinement. The SHELXS97, SHELXL97, and SHELXTL [46] programs were used for all calculations. Atomic scattering factors were those incorporated in the computer programs. Selected interatomic bond distances and angles are listed in table 2 and geometrical parameters of intermolecular interactions are listed in table 3.

3. Results and discussion

Perspective views of structures of **1**, **2**, and **3** with atom numbering scheme are shown in figures 1–3, respectively. Metal (M) to ligand (L) ratio 1 : 1 leads to the formation of one 1 : 2 (M : L) compound (**1**) and two 1 : 1 (M : L) compounds (**2** and **3**). All atoms of all compounds lie in general positions, but **2** and **3** have internal inversion centers at 0.5, 0, 0 (special positions *b* and *d* of the space groups *C*2/*c* and *C*2/*c*, respectively), thus they occupy two asymmetric units. Some nitrate ions and water molecules show symptoms of disorder, manifested in slightly prolating displacement ellipsoids. The magnesium, calcium, and strontium cations are six, eight, and nine coordinated, in agreement with enlarging ionic radius of the metal. The magnesium ion is surrounded only by water molecules, whereas the calcium and strontium ions are coordinated by two chelating nitrate ions, one bridging nitrate ion and water molecules (three and four water molecules, respectively, for **2** and **3**), thus one nitrate ion per each cation is a chelating-bridging trifunctional one and

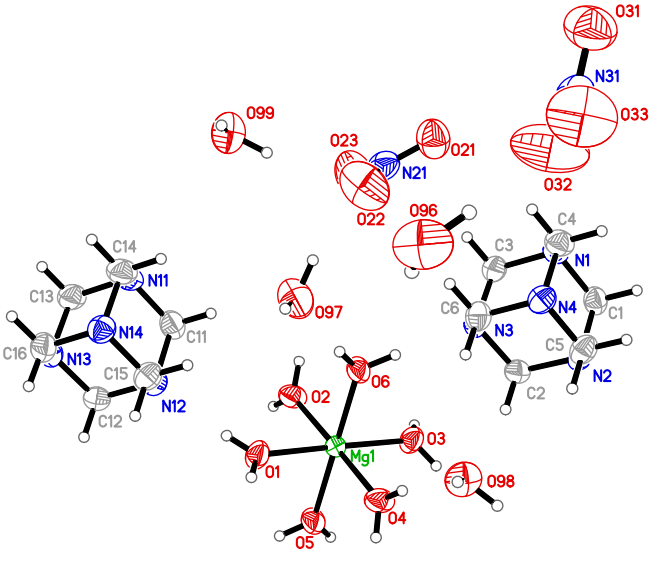

Figure 1. The structure of **1** with atom numbering, plotted with 50% probability ellipsoids. Hydrogen atoms are drawn as spheres of arbitrary radii.

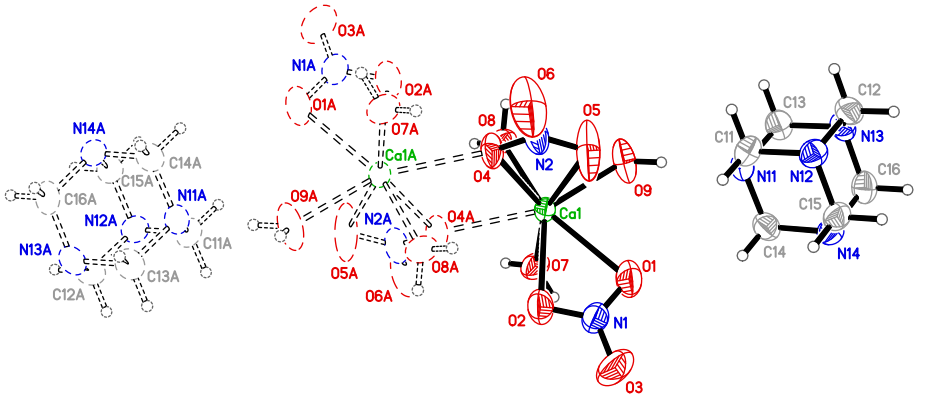

Figure 2. The structure of **2** with atom numbering, plotted with 50% probability ellipsoids. Hydrogens are drawn as spheres of arbitrary radii.

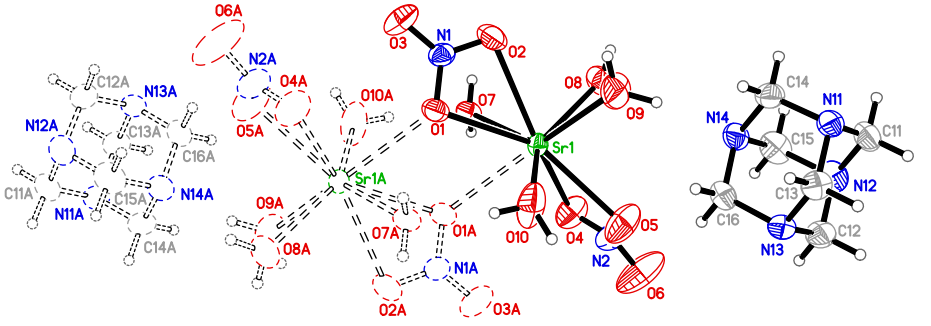

Figure 3. Compound **3** with atom numbering, plotted with 50% probability ellipsoids. Hydrogen atoms are drawn as spheres of arbitrary radii.

the other is a chelating bifunctional ion. Molecules of hmta are located in the outer coordination sphere. Nitrate ions of **2** are unsymmetrically bonded to the calcium cation. In **3**, one nitrate ion is symmetrically bonded and one is slightly unsymmetrically bonded to the strontium cation (table 2). The coordination polyhedra can be described as an almost ideal octahedron, a distorted dodecahedron, and a monocapped square antiprism, strongly distorted towards a tricapped trigonal prism [47–49] (Figure 4). In **1**, all four atoms deviate 0.0009(5) Å from the least squares O1/O2/O3/O4 plane, 0.0092(5) Å from least squares O1/O3/O5/O6 plane and 0.0085(5)–0.0085(6) Å from least squares O2/O4/O5/O6 plane. The magnesium ion derives 0.0083(7), 0.0074(7), and 0.0093(7) Å from above planes, respectively. These internal polyhedral planes form dihedral angles from 87.39(3) to 87.97 (3)° indicating (together with the Mg–O bond lengths) closeness of the coordination environment to ideal polyhedron.

Bond valences were computed as $v_{ij} = \exp[(R_{ij} - d_{ij})/b]$ [50,51], where R_{ij} is the bond-valence parameter (in the formal sense R_{ij} can be considered as a parameter equal to the idealized single-bond length between i and j atoms for given b) and b was taken as 0.37 Å [52–55]. The R_{Mg-O}, R_{Ca-N}, R_{Sr-N} and R_{K-S} were taken as 1.693, 1.967, and 2.118, respectively [56]. The computed bond valences of the metal ions show that the water molecules of **1** and **2** are bonded with comparable strength, slightly weaker bonds are created

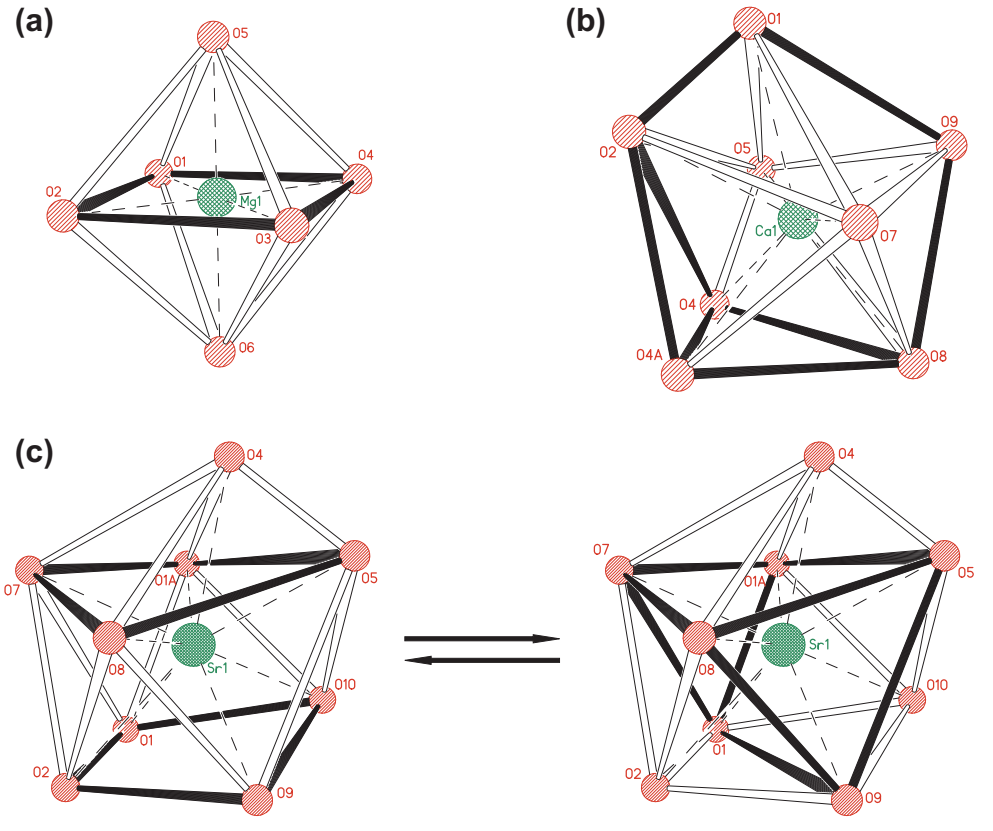

Table 4. Computed bond valences of **1**–**3** [v.u.].

Compound **1**		Compound **2**		Compound **3**	
Mg1–O1	0.385	Ca1–O1	0.223	Sr1–O1	0.197
Mg1–O2	0.380	Ca1–O2	0.277	Sr1–O1^{ii}	0.217
Mg1–O3	0.381	Ca1–O4	0.261	Sr1–O2	0.197
Mg1–O4	0.366	Ca1–O4^{i}	0.245	Sr1–O4	0.213
Mg1–O5	0.368	Ca1–O5	0.181	Sr1–O5	0.239
Mg1–O6	0.376	Ca1–O7	0.351	Sr1–O7	0.280
		Ca1–O8	0.371	Sr1–O8	0.294
		Ca1–O9	0.386	Sr1–O9	0.318
				Sr1–O10	0.325

Symmetry transformations as in table 2

between strontium cation and water molecules of **3**, and the nitrate ion oxygen atoms are the weakest bonded ones in all cases (table 4). In **2** and **3**, bridging M–O bond strengths are between the strengths of chelating M–O bonds and bridging M–O bonds of **2** and slightly weaker than such bond of **3**.

Multiple intramolecular O–H···O, O–H···N and C–H···O hydrogen bonds [57, 58] exist (table 3), creating 3-D networks. Hydrogen bonds are created between nitrate ions, water and hmta molecules and create different graph sets [59–61]. In unitary graph of compound **1**, only D patterns can be found. Chain and ring patterns ($C_2^2(8)$ and $R_4^4(16)$)

can be observed in the binary graph set. There are two $N_2C_2^2(8)$ patterns, created by O–H···N hydrogen bonds formed between magnesium coordinated water molecules and hmta molecules. The four $R_4^4(16)$ patterns, similarly to $C_2^2(8)$ patterns, are created by O–H···N hydrogen bonds (in each N_2R pattern, there are two hmta molecules and two $[Mg(H_2O)_6]^{2+}$ ions). In the unitary and binary graphs, nitrate ions of **1** are engaged only in D patterns, composed of O–H···O hydrogen bonds created between magnesium-coordinated water molecules and nitrate ions. The unitary graph set of **2** is formed by $C_1^1(4)$ $C_2^2(12)R_2^2(12)$ motifs, created by O–H···O hydrogen bonds present between calcium-coordinated water molecules and nitrate ions. The binary graph set consists of $C_2^2(6)$, $C_2^2(8)$, $C_2^2(10)$, $C_4^4(20)$, $R_4^4(16)$, and $R_4^4(20)$ motifs. All are formed by O–H···N hydrogen bonds between calcium-coordinated water molecules and hmta molecules. The unitary graph set of **3** is the most complex, created by one $C_1^1(4)$, $C_2^2(12)$ and $C_2^2(14)$ motifs, two $C_1^1(6)$ motifs and one $R_4^4(20)$, $R_4^4(24)$, $R_6^6(32)$ and $R_6^6(38)$ motifs. All are formed by O–H···N hydrogen bonds between coordinated water molecules and nitrate ions. The binary graph set level of this compound is far more complex and multiple large C and R patterns can be found, e.g. $C_3^3(16)$, $C_3^3(18)$, $R_6^6(36)$ and $R_6^6(38)$.

The IR spectra of the studied compounds exhibit typical, strong bands assigned to hmta. Most of these bands (e.g. at 688–691 and 1383–1384 cm^{-1}) shift to higher frequencies in comparison to pure ligand (table 5). These shifts are caused by O–H···N and C–H···O hydrogen bonds existing between hmta molecules and other molecular and ionic species (table 3). Bands of NO_3^- bending at 735–760 cm^{-1} (**1** and **2**) are distinctly shifted to higher frequencies in comparison to free nitrate ion in solution (table 5), mainly due to immobilization of these ions in the crystal net. In **2**, this vibration is weakened and shifted to lower frequencies in comparison to pure salt, while in **3** this vibration is not observed. This effect originates from existence of the nitrate ions of **2** and **3** in the inner coordination sphere, what diminishes and weakens the force of the respect oscillators. Band of NO_3^- stretching vibrations (at 1370 cm^{-1}) is overlapped with the band of CH_2 wagging vibrations derived from hmta molecules, leading to distinct broadening of the band in comparison to pure salt and hmta. In **3**, the NO_3^- combination bands and overtones are most populated (in comparison to **1** and **2**, table 5) what originates from different nitrate ion bonding to strontium ion (symmetrical and unsymmetrical). In **2**, both nitrate ions are bonded similarly, decreasing the population of overtones, and in **1**, nitrate ions are located in the outer coordination sphere leading to the simplest spectrum. In all spectra, typical bands originating from OH bending and stretching vibrations of water molecules are present at 1650–1680 cm^{-1} and about 3430 cm^{-1}, respectively (table 5).

Thermal decomposition of the investigated compounds is a gradual process (scheme 1) with endothermic multi-step removal of water molecules occurring first. In **1**, decomposition starts at 55 °C and water molecules are removed in two individual steps. First, four water molecules of the outer coordination sphere are released and when the temperature reaches 113 °C, the six ones located in the inner coordination sphere are eliminated. Further heating leads to transformation of $Mg(NO_3)_2$ into MgO with formation of NO_2 and O_2 as gaseous products. Next, exothermic combustion of hmta starts and it is finished at 599 °C. The residue is pure MgO. Dehydration of **2** starts at lower temperature than this of compound **1**, although in **2**, all water molecules are in the inner coordination sphere. Similar to **1**, this is a two-step process, but further decomposition of **2** is different than that observed in **1**. Next is the decomposition of hmta (Scheme 1). During further heating, calcium nitrate decomposes with formation of nitrogen dioxide and oxygen as volatile products

Table 5. Vibrational frequencies [cm^{-1}] and their assignments for **1–3**.

Compound **1**	Compound **2**	Compound **3**	Magnesium nitrate [65]	Calcium nitrate [66]	Strontium nitrate [67]	A dissociated nitrate ion in a solution [68]	Hmta [69,70]	Assignment
3447mbr	3424mbr	3438mbr						υ O–H·(H_2O)
	2965 m	2960w					2966	υ CH
	2936w	2938w					2955	υ CH
	2888w	2889w					2874	υ CH
		2474vw			2490			$^{*}NO_3^-$
2427w	2425vw	2426vw						$^{*}NO_3^-$
	2393vw	2395vw						$^{*}NO_3^-$
2364w								$^{*}NO_3^-$
	2285wbr							$^{*}NO_3^-$
		2248vw			2200			$^{*}NO_3^-$
		2174vw			2171			$^{*}NO_3^-$
		2073vw			2100			$^{*}NO_3^-$
2048w								w O–H·(H_2O)
	2018vw	2019vw						$^{*}NO_3^-$
	1960vw	1957vw						$^{*}NO_3^-$
		1835vw			1867			υ NO_3^-
	1789w	1786vw		1764	1789 & 1794			υ CH, NO_3^- combination band
1680 m	1672w	1653s						δ O–H (H_2O)
	1605 m							δ O–H (H_2O)
		1487vw					1489	s CH_2
1465s	1464s	1463 m					1456	s CH_2
1453vw							1440	s CH_2
1384vs	1383vs	1384vs	1330, 1377		1369		1370	τ CH_2, υ (NO_3^-)
1240vs	1239vs	1238vs					1234	υ CN
1205 m		1207vw						δ N–C–N
1145vs	1148vw							υ CN, δ CH
1095vw								υ CN
1053 m	1044w			1047			1026	υ CN, υ (NO_3^-)
1008vs	1007vs	1009vs					1007	υ CN
939vw		935w						υ CN

(*Continued*)

Table 5. (*Continued*).

Compound **1**	Compound **2**	Compound **3**	Magnesium nitrate [65]	Calcium nitrate [66]	Strontium nitrate [67]	A dissociated nitrate ion in a solution [68]	Hmta [69,70]	Assignment
839vw	836w					830		δ (NO_3^-)
816vw	814s	817s	821, 819	822	812			γ (NO_3^-)
758 m	735w		740, 759	746	741	680		δ (NO_3^-)
691s	688vs	688s					673	δ N–C–N
		646w						δ N–C–N
597w		588w		561				ω O–H (H_2O), ρ O–H (H_2O)
518w		513w					512	τ N–C–N
510 m		503w					510	τ N–C–N

Vibration symbols: vw – very weak, w – weak, m –medium strength, s – strong, vs – very strong, br – broadened, υ – stretching, δ – bending, τ – wagging, ρ – rocking, σ – scissoring, * – overtone, and combination band

$[Mg(H_2O)_6]^{2+} \bullet 2NO_3^- \bullet 2hmta \bullet 4H_2O$
| stage I, m.l. 11.67% / 11.83%; (55 - 113 °C), 102 °C endo
↓ $-4H_2O$
$[Mg(H_2O)_6]^{2+} \bullet 2NO_3^- \bullet 2hmta$
| stage II, m.l. 16.89% / 17.74%; (113 - 164 °C), 137 °C endo
↓ $-6H_2O$
$Mg(NO_3)_2^* \bullet 2hmta^*$
| stage III, m.l. 17.95% / 17.74%; (164 - 234 °C), 196 °C exo
↓ $-2NO_2, -0.5O_2$
$MgO^* \bullet 2hmta^*$
| stage IV, m.l. 47.45% / 46.06%; (234 - 599 °C), 260 °C exo
↓ -2hmta
MgO^*

$[Ca_2(H_2O)_6(NO_3)_4] \bullet 2hmta$
| stage I, m.l. 5.08% / 5.02%; (26 - 87 °C), 60 °C endo
↓ $-2H_2O$
$[Ca_2(H_2O)_4(NO_3)_4] \bullet 2hmta$
| stage II, m.l. 11.69% / 10.05%; (87 - 166 °C), 146 °C endo
↓ $-4H_2O$
$2Ca(NO_3)_2^* \bullet 2hmta^*$
| stage III, m.l. 38.42% / 39.13%; (146 - 337 °C), 216 °C exo, 243 °C exo
↓ -2hmta
$2Ca(NO_3)_2^*$
| stage IV, m.l. 29.80% / 30.14%; (337 - 337 °C), 401 °C exo, 463 °C exo, 570 °C exo
↓ $-4NO_2, -O_2$
$2CaO^*$

$[Sr_2(H_2O)_8(NO_3)_4] \bullet 2hmta$
| stage I, m.l. 11.64% / 12.74%
| stage Ia, m.l. 3.84% / — (98 - 120 °C), 115 °C endo
| stage Ib, m.l. 7.80% / — (120 - 145 °C), 132 °C endo
↓ $-6H_2O$
$[Sr_2(H_2O)_2(NO_3)_4] \bullet 2hmta$
| stage II, m.l. 46.72% / 46.77% (132 – 235 °C), 223 °C endo
↓ $-2H_2O$, -2hmta, $-1.6 NO_2, -0.4 O_2$
$0.8SrO^* / 1.2Sr(NO_3)_2^*$
| stage III, m.l. 6.53% / 5.50%; (235 – 569 °C)
↓ -0.45SrO
$0.35SrO^* / 1.2Sr(NO_3)_2^*$
| stage IV, m.l. 15.93% / 15.29%; (569 - 653 °C), 601 °C endo, 636 °C endo
↓ $-2.4NO_2, -0.6O_2$
$1.55\ SrO^*$

Scheme 1. Stages of the thermal decomposition of the studied compounds, m.l. – experimental mass loss/ theoretical mass loss. * – the product was confirmed by XRPD.

$(2Ca(NO_3)_2 \rightarrow 2CaO + 4NO_2 + O_2)$ [62]. The thermal decomposition ends at 697 °C with the formation of CaO as the final product. **3** is stable to 98 °C (thus it is the most thermally stable compound among the studied ones), then six water molecules are removed in two overlapping but distinguishable substages (Scheme 1). After that, in a quick endothermic process, hmta, together with two remaining water molecules, are removed and the compound decomposes into the mixture of SrO and $Sr(NO_3)_2$ (molar ratio 2 : 3) with the

formation of NO_2 and O_2 as gaseous products. Next, part of the SrO is removed, perhaps by the formation of nanosized and smaller volatile SrO [63]. At the end, $Sr(NO_3)_2$ melts (lit. m.p. of the pure salt is 570 °C [64]) and decomposes to SrO, NO_2, and O_2. The final solid product is SrO, but at 653 °C (when the strontium nitrate decomposition finishes), a small but observable mass loss, up to the limit of measurement (1000 °C), is still observed, what proves that the formed particles of SrO are blown away by air flowing in the thermal analyzer.

4. Conclusion

The reaction of hmta with alkaline earth metal nitrates (magnesium, calcium and strontium) leads to coordination complex compounds. In all cases, the amine ligands are located in the outer coordination sphere but placement of nitrate ions is different, in the outer coordination sphere for lightest metal (compound **1**) and in the inner coordination sphere for heavier metals (compounds **2** and **3**). As a consequence the inner coordination sphere nitrate anions can act as bridging ligands and can form the multinuclear (dinuclear in presented case) complex compounds. The coordination number of metal increases with increasing atomic mass. These structural differences affect the thermal and spectral properties of the compounds. Migration of the nitrate ions from the outer to the inner coordination sphere (and as a consequence formation of dinuclear compound) leads to decreasing thermal stability of subsequent metals (compound **1** vs. compound **2**), while enlargement of the coordination number of metals surrounded by the same types of ligands leads to increasing thermal stability. Increasing of the atomic number leads to "stabilising" of the nitrate ions in the structure (from outer coordination sphere located ones, through the unsymmetrically bonded to the metal atom, to the symmetrically bonded to the metal atom). The introduction of the hmta to the outer coordination sphere allows changing of the inner coordination sphere and, in consequence, obtaining the unique dinuclear coordination compounds of calcium and strontium nitrates.

Supplementary data

Tables of crystal data and structure refinement, anisotropic displacement coefficients, atomic coordinates, and equivalent isotropic displacement parameters for non-hydrogen atoms, H-atom coordinates, and isotropic displacement parameters, bond lengths, and interbond angles have been deposited with the Cambridge Crystallographic Data Centre under Nos. CCDC865230, CCDC865231, and CCDC865232, respectively, for **1**, **2**, and **3**.

Acknowledgments

This work was financed by funds allocated by the Ministry of Science and Higher Education to the Institute of General and Ecological Chemistry, Technical University of Lodz.

References

[1] A. Trzesowska-Kruszynska. *J. Coord. Chem.,* **64**, 663 (2011).
[2] Y.F. Chen, L. Wei, J.L. Bai, H. Zhou, Q.M. Huang, Z.Q. Pan. *J. Coord. Chem.,* **64**, 1153 (2011).
[3] M. Kalanithi, M. Rajarajan, P. Tharmaraj. *J. Coord. Chem.,* **64**, 842 (2011).
[4] Q.J. Kong, M.X. Hu, Y.G. Chen. *J. Coord. Chem.,* **64**, 3237 (2011).
[5] R. Alizadeh, V. Amani. *Struct. Chem.,* **22**, 1153 (2011).

[6] N. Veeraraghavan, A. Ganguly, J.H. Chen, P.C. Bevilacqua, S. Hammes-Schiffer, B.L. Golden. *Biochemistry–US.,* **50**, 2672 (2011).
[7] D. Ali Köse, B. Zümreoglu-Karan, T. Hökelek. *Inorg. Chim. Acta,* **375**, 236 (2011).
[8] B.G. Oliveira, R.C.M.U. Araujo, J.J. Silva, M.N. Ramos. *Struct. Chem.,* **21**, 221 (2010).
[9] L. Botana, R. Bastida, A. Macías, P. Pérez-Lourido, L. Valencia. *Inorg. Chim. Acta,* **362**, 3351 (2009).
[10] M.A. Aldamen, S.F. Haddad. *J. Coord. Chem.,* **64**, 4244 (2011).
[11] A. Huczyński, J. Janczak, B. Brzezinski. *Inorg. Chim. Acta,* **370**, 353 (2011).
[12] Y. Chi, S. Ranjan, P.W. Chung, H.Y. Hsieh, S.M. Peng, G.H. Lee. *Inorg. Chim. Acta,* **334**, 172 (2002).
[13] K. Wieczorek-Ciurowa, P. Dulian, A. Nosal, J. Domagala. *J. Therm. Anal. Calorim.,* **101**, 471 (2010).
[14] D. Banerjee, J. Finkelstein, A. Smirnov, P.M. Forster, L.A. Borkowski, J.B. Parise. *Cryst. Growth. Des.,* **11**, 2572 (2011).
[15] S. Natarajan, J. Kalyana Sundar, S. Athimoolam, B.R. Srinivasan. *J. Coord. Chem.,* **64**, 2274 (2011).
[16] Y. Xiang, J. Du. *Chem. Mater.,* **23**, 2703 (2011).
[17] J.Y. Reginster, E. Seeman, M.C. Vernejoul, S. Adami, J. Compston, C. Phenekos, J.P. Devogelaer, M. Diaz Curiel, A. Sawicki, S. Goemaere, O.H. Sorensen, P.J. Meunier. *J. Clin. Endocrinol. Metab.,* **90**, 2816 (2005).
[18] M.D. O'Donnell, R.G. Hill. *Acta. Biomater.,* **6**, 2382 (2010).
[19] P.G. Daniele, C. Foti, A. Gianguzza, E. Prenesti, S. Sammartano. *Coord. Chem. Rev.,* **252**, 1093 (2008).
[20] A. Gaur, B.D. Shrivastava, D.C. Gaur, J. Prasad, K. Srivastava, S.N. Jhad, D. Bhattacharyya, S.K. Deb. *J. Coord. Chem.,* **64**, 1265 (2011).
[21] Z.L. You, X.L. Wang, J.C. Zhang, C. Wang, X.S. Zho. *Struct. Chem.,* **22**, 1297 (2011).
[22] J.Y. Chen, Y.L. Liu, W.Q. Xu, E.X. He, S.Z. Zhan. *J. Coord. Chem.,* **64**, 2606 (2011).
[23] B.R. Srinivasan, S.Y. Shetgaonkar, N.N. Ghosh. *J. Coord. Chem.,* **64**, 1113 (2011).
[24] A.E. Lapshin, O.V. Magdysyu. *Glass. Phys. Chem.,* **35**, 627 (2009).
[25] M.F. Belian, R.O. Freire, A. Galembeck, G.F. Sa, R.F. Farias, S. Alves. *J. Lumin.,* **130**, 1946 (2010).
[26] H.L. Zhu, J.L. Lin, W. Xu, J. Zhang, Y.Q. Zheng. *J. Coord. Chem.,* **64**, 1088 (2011).
[27] H.G. Bagaria, M.R. Dean, C.A. Nichol, M.S. Wong. *J. Chem. Educ.,* **88**, 609 (2011).
[28] M. Grzelczak, J. Vermant, E.M. Furst, L.M. Liz-Marza. *ACS Nano.,* **4**, 3591 (2010).
[29] A. Sengul, O. Kurt, O. Buyukgungo. *Struct. Chem.,* **22**, 925 (2011).
[30] M.O. Agwara, P.T. Ndifon, M.K. Ndikontar. *Bull. Chem. Soc. Ethiop.,* **18**, 143 (2004).
[31] A. Pizzi, R. Kueny, F. Lecoanet, B. Massetau, D. Carpentier, A. Krebs, F. Loiseau, M. Ragoubi. *Ind. Crops. Prod.,* **30**, 325 (2009).
[32] M.H. Choi, I.J. Chung, J.D. Lee. *Chem. Mater.,* **12**, 2977 (2000).
[33] D. Greenwood, R.C.B. Slack. *Infection,* **9**, 223 (1981).
[34] A. Trzesowska-Kruszynska, R. Kruszynski, M. Zalewicz, T.J. Bartczak. *J. Coord. Chem.,* **63**, 1013 (2010).
[35] A. Biswas, M.G.B. Drew, Y. Song, A. Ghosh. *Inorg. Chim. Acta,* **376**, 422 (2011).
[36] M.G. Looney, D.H. Solomon. *Aust. J. Chem.,* **48**, 323 (1995).
[37] H. Wu, X.W. Dong, H.Y. Liu, J.F. Ma, Y.Y. Liu, J. Yang. *Inorg. Chim. Acta,* **373**, 19 (2011).
[38] P. Szynkaruk, M. Wesolowski, M. Samson-Rosa. *J. Therm. Anal. Calorim.,* **101**, 505 (2010).
[39] R. Keuleers, G.S. Papaefstathiou, C.P. Raptopoulou, S.P. Perlepes, H.O. Desseyn. *J. Mol. Struct.,* **525**, 173 (2000).
[40] A. Trzesowska, R. Kruszynski. *Transition. Met. Chem.,* **32**, 625 (2007).
[41] R. Kruszynski. *Inorg. Chim. Acta,* **371**, 111 (2011).
[42] Powder Diffraction File International Center of Diffraction Data. *12 Campus Boulevard*, New York, NY (1999).
[43] L. Shimoni, J.P. Glusker, C.W. Bock. *J. Phys. Chem.,* **100**, 2957 (1996).
[44] J. Bernstein, L. Shimoni, R.E. Davis, N.L. Chang. *Angew. Chem. Int. Ed. Engl.,* **34**, 1555 (1995).
[45] R. Kruszynski, T. Sieranski. *Cent. Eur. J. Chem.,* **9**, 94 (2011).
[46] S. Yuvaraj, L. Fan-Yuan, C. Tsong-Huei, Y. Chuin-Tih. *J. Phys. Chem. B.,* **107**, 1044 (2003).
[47] T. Sieranski, R. Kruszynski. *J. Therm. Anal. Calorim.,* **109**, 141 (2011).
[48] R. Srinivasan. *Proc. Indian Acad. Sci. A.,* **41**, 49 (1955).
[49] T.G. Chang, D.E. Irish. *J. Phys. Chem.,* **77**, 52 (1973).
[50] J. Hetmańczyk, Ł. Hetmańczyk, A. Migdał-Mikuli, E. Mikuli, K. Druzbicki, L.M. Proniewicz. *J. Chem. Phys.,* **131**, 94506 (2009).
[51] C.J.H. Schutte. *Zeitschrift fiir Kristallographie,* **126**, 397 (1968).
[52] J.T. Kloprogge, D. Wharton, L. Hickey, R.L. Frost. *Am. Mineral.,* **87**, 623 (2002).
[53] M.P. Bernstein, S.A. Sandford, L.J. Allamandola, S. Chang. *J. Phys. Chem.,* **98**, 12206 (1994).
[54] J.O. Jensen. . *Spectrochim. Acta, Part. A.,* **58**, 1347 (2002).